Ain Shams Engineering Journal 16 (2025) 103302

Contents lists available at ScienceDirect

Ain Shams Engineering Journal

journal homepage: www.sciencedirect.com

Crack propagation and CT imaging of internal cracks in rocks damaged by pre-compression under explosive loading

Qiangqiang Zheng [a,b,c,d,*], Pingfeng Li [b,e,*], Ying Xu [a,c], Bing Cheng [a], Hao Hu [c], Hao Shi [a], Shoudong Xie [b,e]

[a] Anhui Engineering Research Center of New Explosive Materials and Blasting Technology of Anhui University of Science and Technology, Anhui University of Science and Technology, Huainan, Anhui 232001, China
[b] Key Laboratory of Safety Intelligent Mining in Non-coal Open-pit Mines, National Mine Safety Administration, Guangzhou 510000, China
[c] State Key Laboratory of Mining Response and Disaster Prevention and Control in Deep Coal Mines, Anhui University of Science and Technology, Huainan, Anhui 232001, China
[d] Laboratory of Seismology and Physics of Earth's Interior, School of Earth and Space Sciences, University of Science and Technology of China, Hefei, Anhui 230026, China
[e] Hongda Blasting Engineering Group Co., Ltd., Changsha, Hunan 410011, China

ARTICLE INFO

Keywords:
Blast loading
Crack propagation
Pre-compression
Fracture zone
CT imaging

ABSTRACT

This study investigates the dynamic crack propagation mechanism in damaged rocks under blasting excavation in complex geological conditions. A novel rock fracture analysis method based on pre-compression-induced random damage is proposed, overcoming the limitations of traditional prefabricated crack models. Innovatively, multi-level cyclic static pre-compression is applied to simulate the random damage distribution in engineering-scale rocks, combined with high-resolution computed tomography (CT) imaging to achieve non-destructive 3D visualization of internal crack morphologies under explosive loading. A theoretical model for predicting blast-induced crack propagation radius in damaged sandstone is established and validated through integrated laboratory blast experiments, CT scanning, and PFC-2D numerical simulations, demonstrating a prediction error margin below 5%. Key findings reveal a significant positive correlation between sandstone damage levels and the expansion range of blast-induced cracks as well as crater dimensions. The pre-existing crack network in damaged rocks effectively guides gas wedging effects, unveiling a "weakening-synergistic fracturing" dual mechanism. These results provide theoretical foundations and technical support for optimizing blasting parameters and mitigating dynamic disasters in tunnel engineering under complex geological settings.

1. Introduction

Tunnel excavation predominantly employs integrated mechanized methods, including shield machines and digging anchor machines [1,2]. However, rock blasting remains essential for excavation in complex geological conditions where integrated mechanization is impractical [3,4]. Concurrently, rocks in regions with complex geological conditions typically sustain varying degrees of damage due to disturbances from mining and tectonic stresses prior to blasting excavation [5,6]. We gain an in-depth understanding of crack propagation within damaged rock subjected to explosive loads and anticipate changes in the stability of the rock surrounding a tunnel during the blasting construction process. This work facilitates the identification of potential areas at risk of collapse, enabling the prompt implementation of support measures, such as enhancing anchor rod support and conducting lining reinforcement [7]. Therefore, in this work we assess ways to effectively mitigate the casualties and property losses that might otherwise result from tunnel collapse incidents.

The rupture of rock under explosive loading is an instantaneous process that is completed in tens of microseconds to milliseconds [8,9]. This process rapidly generates substantial heat, converting solid explosives into high-temperature, high-pressure gases, accompanied by the formation of a blast wave [10,11]. These gases are subsequently consumed in the process of fracturing the rock [12]. The reflected stretching effect theory posits that the detonation wave induces rock deformation and fragmentation [13], whereas the explosive gases

* Corresponding authors.
E-mail addresses: zhengqq@ustc.edu.cn (Q. Zheng), hdbplpf@163.com (P. Li).

https://doi.org/10.1016/j.asej.2025.103302
Received 29 September 2024; Received in revised form 1 February 2025; Accepted 2 February 2025
Available online 8 February 2025

expand and further fracture the rock and eject fragments [14,15]. However, the explosion gas expansion theory suggests that post-explosion energy primarily forces the joints and fissures of the rock, widening and deepening them, thus facilitating rock mass rupture; the detonation wave assists in fracturing and ejecting the rock fragments [16,17]. The lithology, characteristic impedance, and homogeneity of the rock mass underpin the distinctions between these theories [18]. The rupture of highly homogeneous rock masses with characteristic impedance under blast loading is attributed to the reflective stretching effect of the blast wave [19,20]; conversely, this is attributed to the action of explosive gas expansion [21]. Furthermore, the combined effects of the blast wave's reflective stretching and explosive gas expansion are considered crucial to rock rupture under explosive loading [22]. Regardless of the theory, cracks are critical in facilitating rock breakage under explosive loading [23]. Following explosive initiation, fissures in rock serve as diffusion paths for the pneumatic wedging of explosive gases [24]. Conversely, the leakage of high-temperature and high-pressure gases from cracks diminishes their rock-breaking efficacy [25]. However, such leakage is limited to joints at the free surface or penetrating fractures, not to cracks unconnected to the free surface. Constrained by the narrowness of the tunnel's free surface and the extensive impact of explosive loading, cracks induced by mining disturbances within the rock mass are less connected to the free surface [7]. Consequently, cracks created by excavation and tectonic stresses serve as diffusion paths for the pneumatic wedging of explosive gases, thereby weakening the rock mass's strength [26].

Defects such as cracks and joints are intricately distributed within the disturbed rock mass, undeniably affecting the degree of rock fracture under explosive loading [27]. Numerous scholars have investigated the dynamic response of jointed rock masses under explosive loading, yielding valuable research findings [28,29,30]. The number and orientation of joints significantly influence the degree of rock fragmentation following blasting [31,32]. Quantitatively, a greater number of joints correlates with increased rock fragmentation after explosive loading [33,34]. However, the dynamic response of fissured rock under explosive loading is more complex; for example, fragmentation is more uniform when joint surfaces are parallel or at an acute angle to the free surface [35,36]. The shape of the blasting crater and the rock fragmentation process are also influenced by the distribution of joints [37]. Indeed, joints and fissures, as weak surfaces, are prone to crack at stress concentration points under blast loading, and the redistribution of the stress field inevitably alters crack extension [38]. However, defects originating from mining disturbances are randomly distributed and not prefabricated in rock masses—a fact previously overlooked in studies [39]. Additionally, the ratio of prefabricated fissure size to specimen size does not align with that in jointed rock masses used in geotechnical engineering, rendering the results overly conservative [40].

To address the aforementioned shortcomings, this study employs pre-compression on rock samples to achieve varying degrees of damage, ensuring that the damage is randomly distributed within the rock, rather than being prefabricated. A blast load is subsequently applied to the damaged rock samples to investigate the fracture expansion dynamics under explosive loading. CT is utilized to observe the internal fracture expansion patterns in rock, overcoming the limitations of other monitoring methods that capture only surface crack expansion. Numerical simulations are then used to verify crack propagation in rocks damaged by pre-compression under explosive loads. The findings of this research are intended to offer more precise blasting parameters, enhanced protective designs, and effective disaster prevention and control strategies for blasting construction projects.

2. Theoretical analysis

Shock waves, generated by explosives detonating within rock rapidly attenuate into stress waves. Upon the application of stress waves, compressional and tensile deformations are induced separately in the radial and tangential directions of the rock. According to rock mechanics theory, the tensile capacity of rock is low. Consequently, cracking occurs where the tangential tensile stress exceeds the rock's dynamic tensile strength. The conditions for rock cracking are detailed in Eq. (1) [41]. Furthermore, the attenuation of pressure from the stress wave as it propagates through the rock is described in Eq. (2) [41].

$$\sigma_\theta > \sigma_{dt} \tag{1}$$

$$\sigma_r > \frac{P_r}{\bar{r}^{\alpha}} \tag{2}$$

where σ_θ is the tangential tensile stress, MPa; σ_{dt} is the dynamic tensile strength of the rock, MPa; $\bar{r} = r/r_b$, where r is the radial distance from the source of the explosion, m; r_b is the radius of the borehole, m; P_r is the initial radial stress peak, MPa; α is the stress wave attenuation index; and $\alpha = 2 - (\mu_d/(1 - \mu_d))$ [42],$\mu_d = 0.8\mu$, where μ is the static Poisson's ratio, which is measured as 0.28 in this study. Although the value of μ may vary for rocks with different damage levels, the resulting error in Eqs. (2) and (3) can be negligible. Here, it is assumed that the Poisson's ratio of sandstone is not affected by cyclic static loads.

The tensile stress generated in the tangential direction of the rock at r is σ_θ as shown in Eq. (3) [41].

$$\sigma_\theta = \lambda\sigma_r = \lambda\frac{P_r}{(r/r_b)^{\alpha}} \tag{3}$$

where λ is the lateral pressure coefficient, $\lambda = \mu_d/(1 - \mu_d)$.

Considering the varying dynamic tensile strengths of rocks with different degrees of damage, the radius of the fracture zone in damaged rock under blast loading, as defined in Eq. (4), is derived by combining Eqs. (1) and (3).

$$R_s = r_b\left[\frac{\lambda P_r}{\sigma_{dt\beta}}\right]^{\frac{1}{\alpha}} \tag{4}$$

where R_s is the radius of the fracture zone, m, and where $\sigma_{dt\beta}$ is the dynamic tensile strength of the rock at damage level β.

In this study, the explosive stress damage zone is used to predict the extent of rock damage under explosive loading, considering initial damage. The blasting parameters, dynamic tensile strength, and dynamic Poisson's ratio of the rock are used to define the explosive damage zone, which in turn informs blasting engineering practices.

3. Experimental methodology

3.1. Materials and experimental equipment

This study investigated the fracture zone of damaged rock under explosive loading. The rocks, specifically sandstone, were excavated in situ from an open-pit mine in Zhoushan city, China. After cutting and polishing, rectangular samples measuring 220 mm × 220 mm × 50 mm were prepared, and a borehole with a depth of 30 mm and a diameter of 10 mm was drilled at the geometric center of the end face to facilitate the blasting tests. Moreover, in contrast to traditional methods of estimating rock damage by damage factors, this study employs the Split Hopkinson Pressure Bar (SHPB) to measure the dynamic tensile strength of rocks damaged by static loads. Consequently, cylindrical sandstone samples 50 mm in diameter and 25 mm in height were prepared for measuring the dynamic tensile strength. In accordance with guidelines from the International Society for Rock Mechanics (ISRM), the end face roughness was maintained at less than 0.5 % of the sandstone thickness.

In this study, loading devices capable of applying a range of strain rates from static (low strain rates) to explosive (high strain rates), along with other related instruments, were utilized. A mechanical testing and simulation (MTS-816) apparatus was used to perform the static load tests. Most notably, the application of static loads serves as one method

aimed at inducing varying degrees of damage in sandstones. A 50 mm diameter SHPB device made of high-strength maraging steel with a Young's modulus of 210 GPa and density of 7900 kg/m^3, was employed to determine the dynamic tensile strength of the damaged rock. A self-manufactured compressed Hexogen (RDX) explosive was used in a detonator for explosive loading tests on damaged rock. Furthermore, a microfocus CT scanner equipped with a 300 kV/500 W microfocus ray tube was employed to capture the extension of fractures in the rock following explosive loading.

3.2. Experimental process

The fracture zone test for damaged rock under explosive loading sequentially covers low, medium, and high strain rates, progressing from static loading to impact loading to explosive loading. First, MTS-816 was used to determine the static compressive strength of the rock σ_b, and against this background, cyclic loads with upper limits of 0.2 σ_b, 0.4 σ_b, 0.6 σ_b, and 0.8 σ_b were applied to the sandstone samples to ensure diverse damage levels. Importantly, two sizes of rock samples were employed: a 50 mm diameter by 25 mm thick sample for measuring the dynamic tensile strength and a 220 mm × 220 mm × 50 mm sample for the blast loading tests. For both types of samples, the quantity of loading–unloading cycles is precisely 6. Owing to the large length–to–span ratio of the sandstone samples, the strength exceeded the loading range during the test, with a side length of 50 mm in the axial direction. Therefore, cyclic loading tests were performed with a side length of 220 mm in the axial direction to accommodate damage-induced static loading. The SHPB was subsequently used to conduct impact loading tests on sandstone samples at various damage levels to measure their dynamic tensile strength. Homemade compressed 0.6 g RDX explosives were used for blast mechanics tests on sandstone at various damage levels, followed by CT scanning to image and analyze the fracture zones post-explosion. Notably, before plugging the borehole, the interior impurities must be cleared. The detonator was vertically fixed without eccentricity via glue. Finally, boreholes are fully filled with equal amounts of stemming, thus enabling as much explosive energy as possible to be exerted on the rock. Additionally, numerical simulations utilizing Particle Flow Code-2 Dimension (PFC-2D) were conducted to validate the experimental findings. The main experimental apparatus and experimental process of this study are shown in Fig. 1.

4. Experimental results

4.1. Basic mechanical parameters of the damaged rock

Understanding the basic dynamic mechanical properties of rocks is fundamental to studying crack propagation in rocks under explosive loads. Following impact compression and tensile tests, the dynamic compressive and splitting tensile strengths of sandstone at varying degrees of damage were determined, as detailed in Table 1.

According to the experimental results, the primary wave velocity, Young's modulus, uniaxial compressive strength, and both dynamic compressive and splitting tensile strengths of sandstone decrease with increasing damage degree. This decrease in strength is attributed to the attenuation of stress waves caused by weak planes in the rock following static loading, a phenomenon corroborated by numerous studies [7,43].

4.2. Characterization of the degree of damage to sandstone samples

After pre-loading to various upper limits, sandstone samples exhibit different degrees of damage. To assess this damage, a non-metallic ultrasonic detector is utilized. Five collection points are established along the edge length on each side of the sandstone sample to measure the wave velocity, which is subsequently averaged. The final average wave velocity, which represents a consistent degree of damage across the samples, is determined and defined as the wave velocity of the damaged sandstone. The initial longitudinal wave velocity, denoted as C_0, and the longitudinal wave velocity of the damaged sandstone, denoted as C, are derived from stress wave theory, as detailed in Eqs. (5) and (6). By utilizing rock damage theory and wave velocity measurements, the damage factor of sandstone under a pre-applied static load can be calculated according to Eq. (7). The damage factors for sandstone subjected to various static load applications are presented in Table 2.

$$C_0 = \sqrt{\frac{E_0(1-\mu)}{\rho(1-2\mu)(1+\mu)}} \tag{5}$$

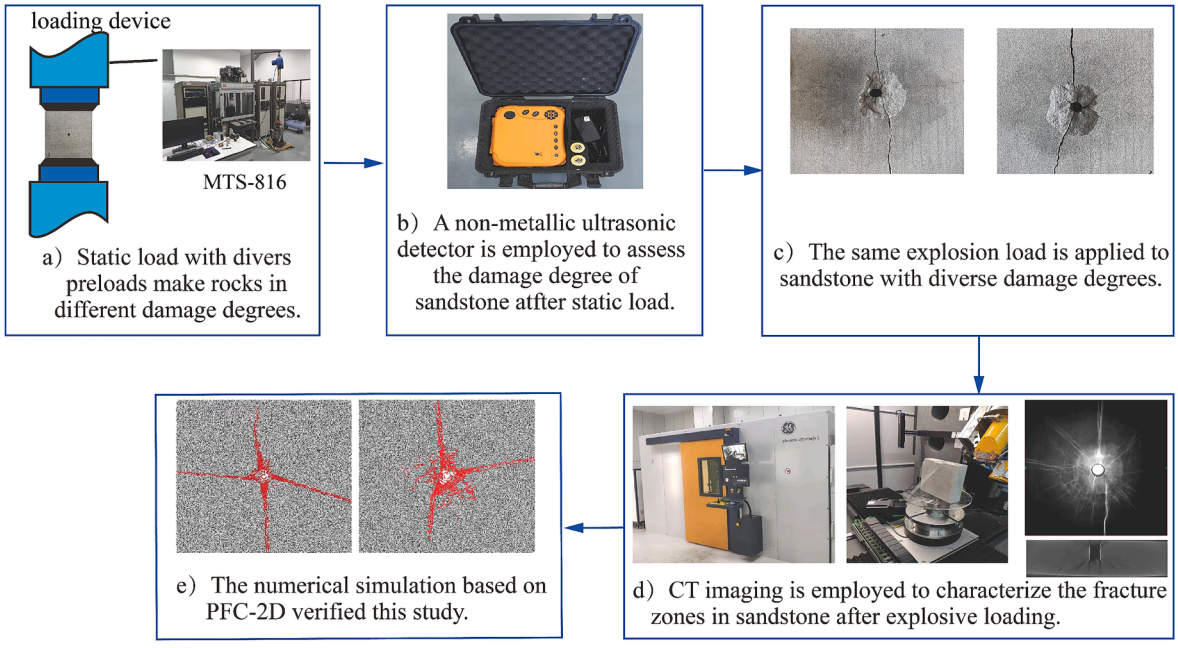

Fig. 1. Main experimental apparatus and experimental process. **Note**: SHPB tests are employed to measure the dynamic strength of sandstone for the theoretical study of fracture radius and are not described in Fig. 1.

Table 1
Dynamic mechanical properties of rock samples with different degrees of damage.

	Primary wave velocity (m/s)	Young's modulus (GPa)	Uniaxial compressive strength (MPa)	Dynamic compressive strength (MPa)	Dynamic splitting tensile strength (MPa)
0	3095	21.42	62.68	65.07	8.52
0.2 σ_b	3050	20.80	61.89	62.90	8.32
0.4 σ_b	2998	20.10	60.71	60.73	7.70
0.6 σ_b	2889	18.67	58.53	54.12	5.21
0.8 σ_b	2618	15.33	51.05	45.98	3.02

Table 2
Damage factor of sandstone after pre-loading with different upper limits.

	0	0.2 σ_b	0.4 σ_b	0.6 σ_b	0.8 σ_b
D′	0	0.0289	0.0617	0.1283	0.2844

$$C = \sqrt{\frac{E(1-\mu)}{\rho(1-2\mu)(1+\mu)}} \tag{6}$$

$$D' = 1-\left(\frac{C_0}{C}\right) \tag{7}$$

where μ is the Poisson's ratio of sandstone; ρ is the density of sandstone, kg/m^3; E_0 and E are the elastic moduli of undamaged sandstone and damaged sandstone, respectively, GPa; and D′ is the damage factor of damaged sandstone.

4.3. Expansion of cracks in damaged rock under explosive loading

The fracture states of sandstones with diverse degrees of damage after explosion loading are shown in Fig. 2.

Differences in crack propagation on the surface of sandstones with varying degrees of damage after being subjected to explosive loads are observed. As the degree of damage in the sandstone increases, both the length and thickness of surface crack propagation under explosive loading also increase. However, the size of the blasting crater on the upper surface of the sandstone remains largely unaffected by explosive loading. Conversely, significant compression deformation occurs at the bottom of the sandstone within the blasting crater, and the extent of fracturing is positively correlated with the degree of damage induced by pre-static loading, as illustrated in Fig. 3.

The fracture patterns of damaged sandstone under explosive loading were analyzed via data from Figs. 2 and 3. In non-damaged sandstone, the upper surface exhibits few cracks, with blast pits as the predominant feature, whereas the extent of cracks formed at the bottom post-blasting remains relatively minor. However, with increasing damage to sandstone, both the scale and extent of surface fractures on the upper surface noticeably increased. Additionally, the degree of rock fracturing at the bottom of the blasting crater intensified. Notably, this study employed inverse initiation, resulting in significantly greater fragmentation at the bottom than at the top, due to the columnar charge and thin sandstone samples, whereas the upper part showed less evident fragmentation.

Additionally, to visually assess the impact range and degree of compression deformation at the bottom of the sandstone after blasting, we measured the compression deformation diameter. The final measurement was determined by the maximum diameter of the deformation and the radius theoretically calculated from Eq. (4), as detailed in Table 3.

The damage at the bottom of the sandstone following the explosive

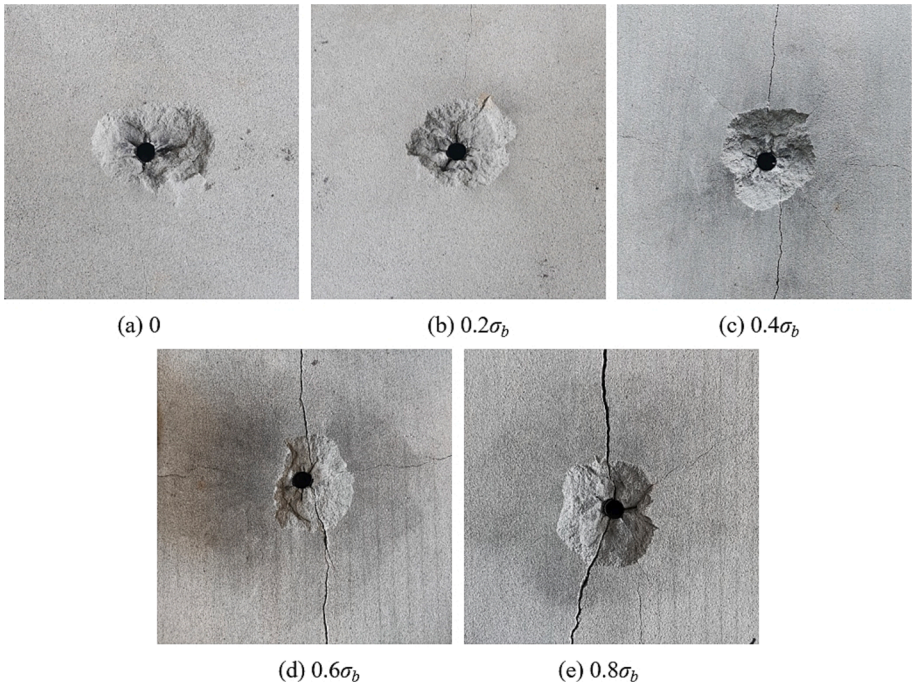

Fig. 2. Fracture states of sandstones with various degrees of damage after explosion loading.

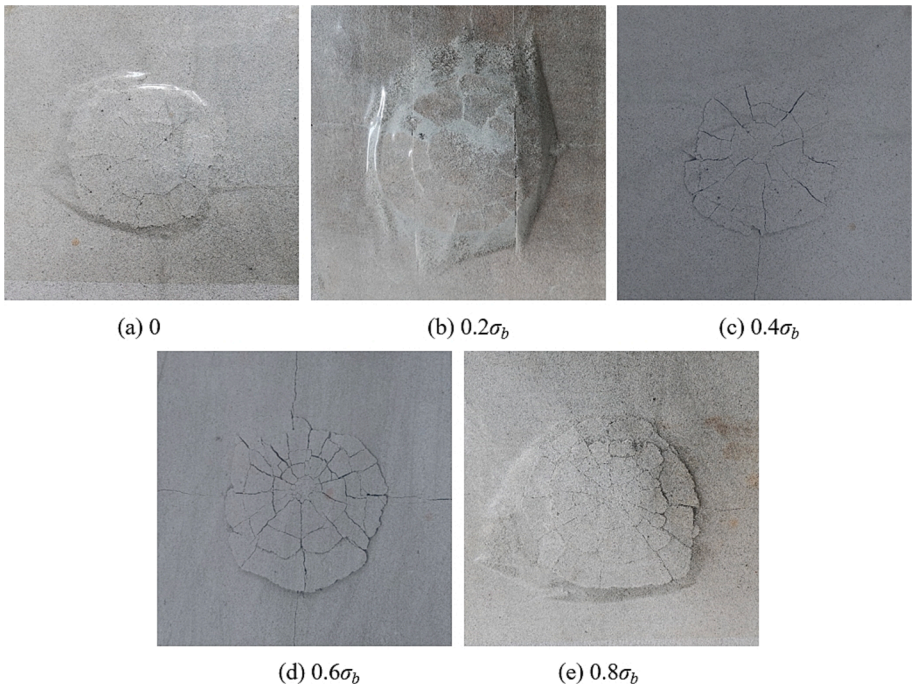

Fig. 3. Fracture shape of bottom blasting craters of sandstone with different degrees of damage under a blast load.

Table 3
Maximum radius of the bottom compression deformation area and the theoretically calculated radius of sandstone after blasting (unit: mm).

	0	0.2 σ_b	0.4 σ_b	0.6 σ_b	0.8 σ_b
R_s	56.95	59.60	72.82	112.53	195.86
$\overline{R}$	59.28	62.38	76.63	>110	>110

load is documented in Fig. 3 and Table 2. The expansion, scale, and extent of the fractures in the planar range are clearly visible. The scale of the protruding fractured rock blocks in the lower sections of the sandstone is also observable. We employ the more intuitive average diameter method to analyze the area affected by compression deformation at the bottom of the sandstone. Using the average diameter of the compression deformation area at the bottom of the intact sandstone sample as a reference, the average diameter increases with the upper limits of the pre-applied static load at 0.2 σ_b and 0.4 σ_b, resulting in increases of 5.23 % and 29.27 %, respectively. The errors between the theoretical calculations and actual measurements are 3.93 %, 4.46 %, and 4.97 %, respectively. It is apparent that the rate of increase accelerates. Unfortunately, when the upper limit of the static load exceeds 0.6, both the theoretically calculated and the measured fracture radii exceed the dimensions of the sandstone sample, which is influenced by the explosive charge and the limitations of the CT scan. However, relying solely on the

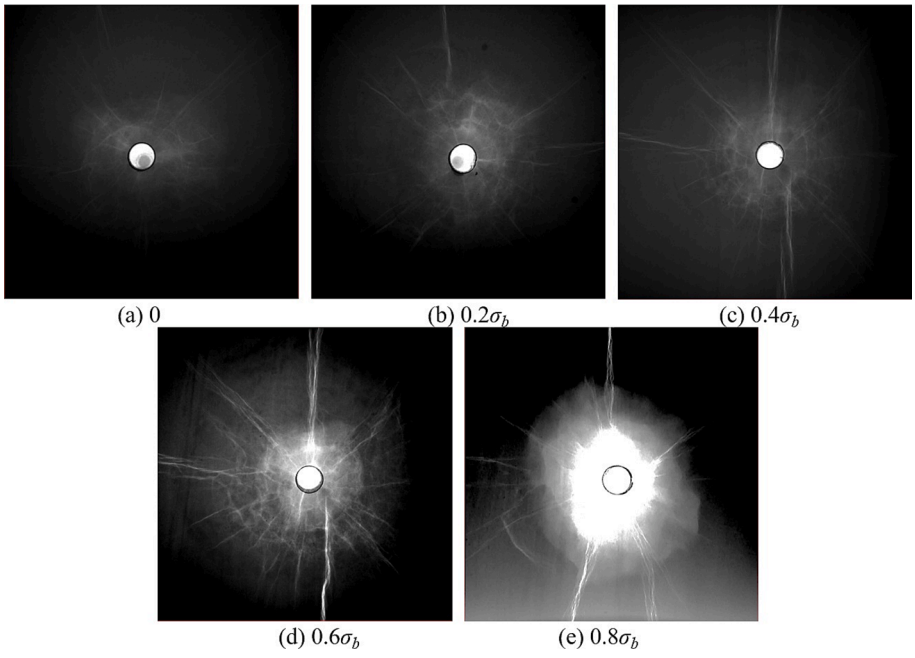

Fig. 4. CT images of diverse damaged sandstone samples with diverse degrees of damage under blast loading.

range of the compression deformation zone at the bottom of the sandstone does not allow for a comprehensive characterization of the internal crack expansion and severity in the damaged sandstone under explosive loads. In addition to the average diameter, factors such as the size and extent of cracks must also be comprehensively considered.

4.4. CT imaging of damaged sandstones under explosive loads

CT scans were performed on each sample after blasting to assess the internal damage and fracture characteristics following the explosive load. CT images depicting the lateral blasting crater and middle cross-sections of sandstone samples with varying degrees of damage under blast loading are presented in Figs. 4 and 5, respectively.

The CT imaging results not only confirmed the accuracy of Figs. 4 and 5 but also revealed fracture ranges that are not directly visible in the rock. CT imaging demonstrated that the degree of damage, the area affected, and the extent of fractures in sandstones under explosive loads increase progressively with the degree of damage. Similarly, the width and length of longitudinal cracks along the edges increase as the degree of damage increases. Compared with other damaged samples, non-destructive sandstone samples exhibit less damage under explosive loads. Slight damage is evident around the borehole, whereas areas beyond half the distance to the boundary remain nearly intact. As depicted in Fig. 4(a), relatively few cracks are generated, with most spreading radially around the borehole. The interlocking of cracks of varying orientations is minimal, with only a few narrow cracks extending towards the boundary. These cracks do not connect or penetrate the damaged area around the borehole, and their impact on the original rock is minimal. Additionally, both the extent of damage and the radius are the smallest, as shown in Fig. 4.

The primary pores in the sandstone, subjected to a static load upper limit of 0.2 σ_b, are compacted and closed, resulting in the formation of no large cracks. Larger solid mineral particles within this sandstone may also promote the formation of small cracks due to the tip effect following static loading. However, the impact of these weak surfaces or cracks on the explosive load is minimal when they are distant from the borehole. Even in proximity to the blast hole, the impact remains limited. Figs. 4 and 5 show that the damaged sandstone subjected to a static load upper limit of 0.2 σ_b has a slight increase in damage range and degree under blasting loading, along with a modest increase in damage radius; however, these increases are still less significant than those in the final three stages. In the vicinity of the borehole, the number of cracks and the scale and number of intersecting cracks both increase. Additionally, two small cracks propagate outwards, parallel to the edges of the rectangle.

When the static load reaches an upper limit of 0.4 σ_b, the tip effect of the mineral particles in the damaged sandstone promotes the formation of randomly distributed cracks within the cementitious matrix. Unlike those in the previous stage, the cracks in this stage are randomly distributed and not influenced by the compaction and closure of larger pores. The cracks that formed in the previous stage, owing to the compaction and closure of primary pores, further expand and weaken in this stage. With the action of the explosive load, the expansion of these cracks is significantly more pronounced than that in the previous stage, as depicted in Fig. 4(c), with both the extent of damage and the radius being greater than those in the initial two stages. As shown in Fig. 4(c), more cracks have formed, and their widths have increased. Most of the cracks radiate from the borehole, and the degree of interlocking among cracks of various orientations is also greater than that in the first two stages. Additionally, more cracks extend towards the boundary of the sandstone sample than in the initial stages do, forming connections with the damaged area at the center of the borehole.

As the upper limit of the static load increases, both the size and number of cracks in the sandstone increase. Particularly when the static load exceeds 0.6 σ_b, the sandstone approaches the plastic stage, with the number and size of cracks accelerating at a rate surpassing those of the initial four stages. Consequently, under the action of explosive loads, the number and size of cracks radiating from the borehole increase, along with a greater degree of interlocking among cracks of various orientations, as depicted in Fig. 4(d). Owing to the penetration of larger cracks around the borehole, the fragmented rock blocks form powder-filled cavities, as illustrated in Fig. 4(e).

5. PFC numerical simulation

5.1. Particle bonding model

PFC-2D, a well-established discrete element particle flow software, has been extensively applied in rock mechanics research. It treats rocks as a set of rigid particles, and the mechanical response of rocks under load is manifested by changes in the contact state between particles [44]. The particle state is governed by the equation of motion (which describes the state of the particles), basic mechanical constitutive relationships (the force–displacement/rotation relationships between particles), and yield criteria (determines the occurrence and type of bond failure). In this study, the bonded particle model (BPM) was adopted [44]. This model combines the contact bonds and parallel bonds available in PFC, as depicted in Fig. 6 [44].

5.2. Calibration of sandstone micro-parameters

It is necessary to determine the model parameters after establishing the computational model in PFC-2D. As mentioned in the previous section, the basic units of the PFC model are the particles and the bonds between them. Therefore, the calibration of mesoscopic parameters mainly involves determining the physical and mechanical properties of these two elements. However, it is extremely difficult to obtain these

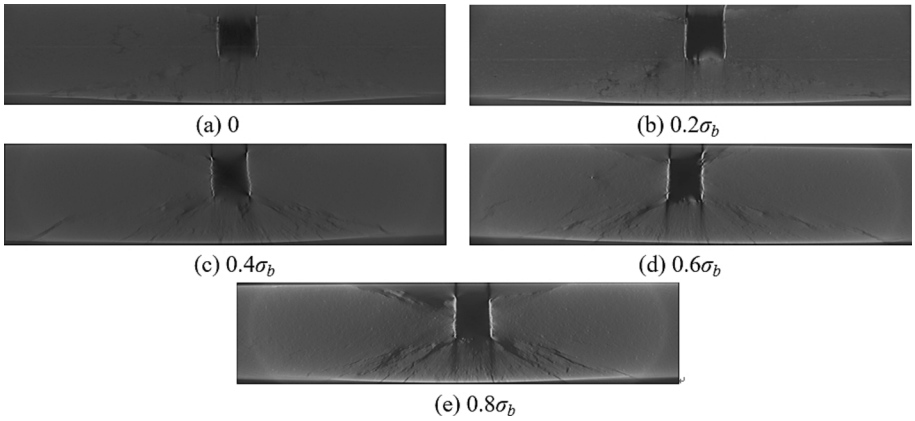

Fig. 5. CT images of the lateral blasting craters of sandstone with diverse degrees of damage under blast loading.

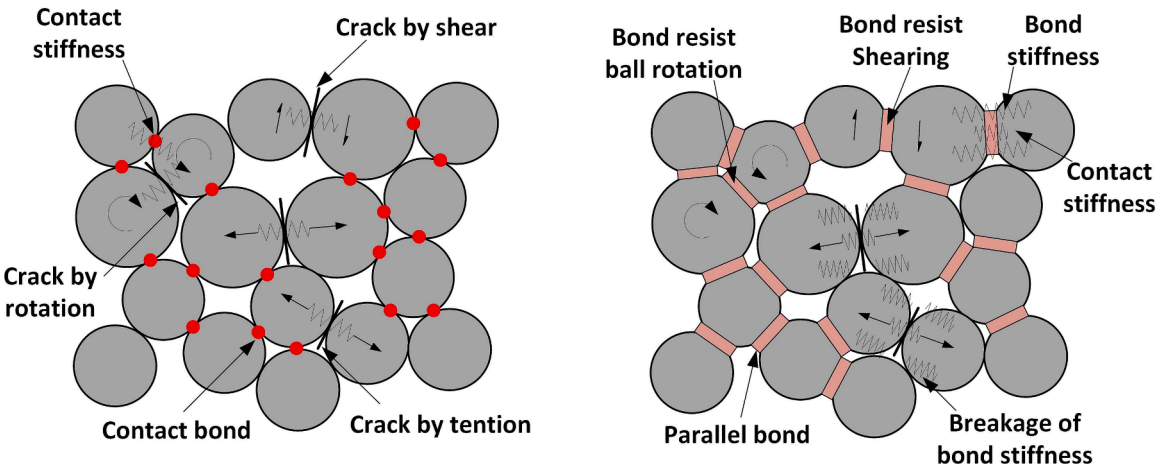

Fig. 6. Two types of key forms in the BPM [44].

parameters directly from experiments. Researchers typically select the full stress–strain curve and corresponding failure mode of a sample as a reference based on experiments [45]. They then use the "trial-error method" to continuously adjust the mesoscopic parameters until the simulated full stress–strain curve and failure mode match the experimental results [45]. At this point, the determined parameters can accurately reflect the physical and mechanical properties of the actual sample and can serve as the basic parameters for further research [46].

The basic mechanical parameters of the rock can be determined based on the sandstone samples and experimental results used in this study. The mineral composition can be found in Zheng et al. [39]. The basic structural parameters of the model are established based on the test dimensions and basic mechanical parameters of the sample. The same loading method and rate as those used in the actual experiment are subsequently set, and the "trial-error method" is employed to determine the microscopic parameters of the calculation model. The mesoscopic parameters of sandstone obtained through calibration are shown in Table 4.

5.3. *The process and results of the numerical simulation*

Based on the determined microscopic parameters of sandstone and referring to the experimental process in Section 3.2 of this paper, six cycles of loading–unloading tests with upper limits of 0.2 σ_b, 0.4 σ_b, 0.6 σ_b, and 0.8 σ_b were carried out on sandstone samples to subject them to varying degrees of damage. For the explosion load test, this study adopts the particle instantaneous expansion method to simulate the blasting loading process [47]. The strain rate of particle expansion is set equal to the strain rate of the explosive used in this study during the explosion. Explosion load simulation tests were conducted on sandstone samples with different degrees of damage via this method, and the test results are presented in Fig. 7.

The numerical simulation results presented in Fig. 7 also validate the accuracy of the theoretical analysis findings. Consistent with these findings, as the degree of sandstone damage increases, the number, size, and expansion radius of cracks in the damaged sandstone under explosive loading, as well as the size of the cavity around the borehole, also increase. The numerical simulation results demonstrate a high degree of consistency with the experimental outcomes. Specifically, the mechanism of sandstone fracture propagation under explosive loading is found to be consistent with that of the indoor experiments, as detailed in Chapter 4.

Table 4
Mesoscopic parameters of the PFC-2D medium.

Parameters	Value	Parameters	Value
Minimum particle size (mm)	0.10	Coefficient of friction	0.66
Maximum particle size (mm)	0.30	Parallel bonding tensile strength (MPa)	26.50
Density (kg·m^{-3})	2390	Parallel bonding cohesion (MPa)	32.00
Porosity	0.15	Parallel bonding friction angle (°)	32.50
Contact adhesion modulus (GPa)	0.50	Parallel bond modulus (GPa)	8.70
Contact adhesion stiffness ratio	1.00	Parallel bonding stiffness ratio	1.00

6. Discussions

This study presents an in-depth theoretical analysis of crack propagation within damaged sandstone subjected to explosive loading and effectively verified the reliability of the theoretical analysis by integrating indoor experiments and numerical simulations. The results reveal a significant positive correlation between the degree of sandstone damage and internal crack propagation after the application of the explosive load. This finding offers crucial references for various aspects, including the design of blasting parameters such as borehole arrangement, charge quantity, and detonation sequence, as well as the design for protecting the stability of rock structures and preventing and controlling dynamic disasters within the mining area.

There is currently no consensus on whether cracks in rock masses under explosive loads are beneficial or detrimental to the effectiveness of rock breaking by blasting. Scholars hold differing views on whether the presence of cracks leads to a premature release of explosive gas, causing energy loss [48], or whether it contributes to the gas wedge effect, thereby promoting rock breakage [10]. The fracture of a rock mass under explosive loading is influenced by lithology, explosive performance, blasting parameters, and occurrence conditions and results from complex, multifaceted interactions [49].

The application of preloading induced local stress concentrations within the rock matrix, which promoted the initiation and subsequent propagation of cracks in the rock. During the crack propagation process, cracks of varying orientations and spatial locations interact synergistically, culminating in the formation of a more complex crack network system [50]. As the upper limit of the static load was incrementally increased, both the magnitude and amount of crack initiation increased. Upon applying explosive loads to the damaged sandstone, the existing cracks functioned via pre-static loading as conduits for disseminating detonation gas pressure; this enables the high-pressure detonation gas to exert a more efficacious influence on rock breaking, thereby exacerbating the extent of damage inflicted upon the rock [51]. Moreover, the cracks that emerged within the rock as a consequence of static loading undermined the overall strength and structural integrity of the rock

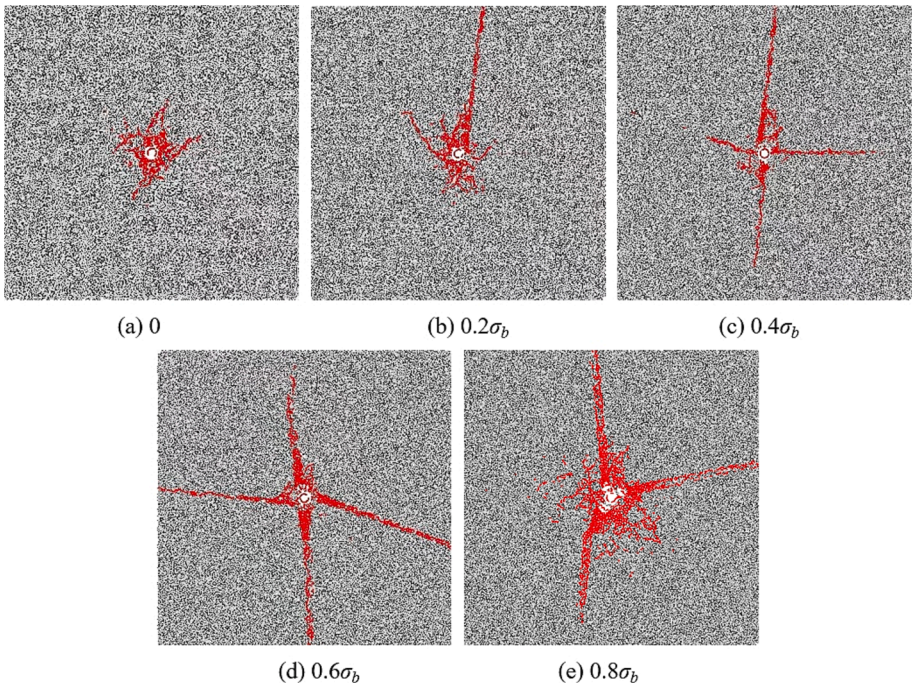

Fig. 7. Numerical simulation results of sandstone with diverse degrees of damage under blast loading.

[52]. Consequently, when detonation gases were introduced, the rock exhibited a heightened susceptibility to damage. Although the internal cracks in the rock affected the propagation of the explosive stress waves, notably, the thickness of the cracks generated by post-static loading was relatively small. This characteristic curtailed their overall influence on the propagation of the stress waves. Additionally, the tensile forces exerted by the stress waves on the weak planes within the rock were conducive to the fragmentation of the rock [53]. A particularly favorable aspect was that most of the cracks that emerged following static loading were located within the rock interior; coupled with the satisfactory level of borehole blockage, this ensured that the detonation gas was effectively retained to break the rock, precluding the occurrence of gas leakage.

It is undisputed that internal rock damage impacts the effectiveness of explosive loads in breaking rocks, which is the primary focus of this study. The impacts of loading methods, cycle numbers, and other factors on the damage level [50], despite their influence, are not considered in this study. However, as we aim to investigate the dynamic mechanical properties of damaged rock, why do we not choose the simplest approach of using static loading to obtain damaged rock? The varying upper limits of cyclic static loading in this study represent one method to achieve different degrees of damage in sandstone; however, the influence of the number of cycles is not addressed. Pre-static loading results in a random distribution of damage within sandstone, more closely simulating the condition of disturbed rock masses in engineering applications. Our method significantly outperforms approaches that use prefabricated crack samples, where the ratio of cracks to specimen size is not representative of actual engineering conditions [8]. However, the direction of pre-static loading plays a crucial role in the penetration of cracks in rock under explosive loads, as illustrated in Fig. 8. According to rock mechanics theory, cracks are generated along the loading direction when a uniaxial load is applied due to friction between the sample end and the loading device [7]. Exploded gas, generated by the load, expands outwards along preloading-induced cracks from the borehole, fracturing the rock, as shown in Fig. 8. Thus, damage to the joints and fissures within the sandstone facilitates the expansion of explosive gas, enhancing rock breakage from this perspective. Consequently, greater damage levels result in more and larger cracks in the sandstone post-explosion, and correspondingly larger blasting craters.

Our study focused on the fracture range of sandstone with varying

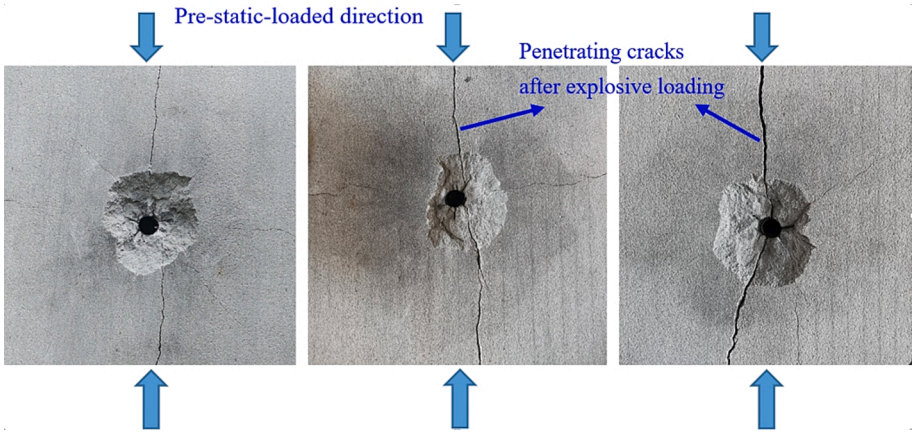

Fig. 8. Influence of the pre-static load direction on crack penetration under explosive loading.

degrees of damage under explosive loads. Unlike traditional measurement methods, we employ CT imaging to characterize the internal fracture range of sandstone. Nevertheless, the micro-nano CT scanner in the laboratory imposes certain size requirements on the scanned samples. If the maximum side length of the sample is excessive, X-rays will be unable to penetrate, preventing the completion of scanning. Therefore, we endeavored to select the largest possible specimen size while ensuring that the samples could be fully scanned. After various sample sizes were tested, we ultimately selected sandstone samples with a maximum side length of 220 mm. Consequently, this limitation results in cracks penetrating sandstone samples under specific explosive loads when the static load exceeds 0.4 σ_b, making quantitative characterization challenging. Furthermore, we employed inverse initiation in this study, resulting in significantly greater fragmentation at the bottom than at the top due to the columnar charge and thin sandstone samples; however, this has a limited influence on the experimental outcomes and does not alter the overall trend observed. Future studies should consider rock thickness and lateral friction forces from preloading to more accurately evaluate the fracture range of damaged rock under explosive loading.

According to the theory of rock mechanics, factors such as lithology, specimen size, and explosive charge can influence the test results of this study. More crucially, it is vital to address the conflict between specimen size and CT scanning for specimen size. Consequently, future research should place greater emphasis on large-scale and even in-situ explosion load tests. Moreover, high-precision imaging methods have been developed to explore crack expansion in rock masses after the application of explosion loads.

7. Conclusions

We theoretically deduced the fracture radius of sandstone featuring varying degrees of damage under explosive loads. Subsequently, CT imaging and numerical simulation were utilized in tandem to corroborate the outcomes of the theoretical analysis. The main conclusions are as follows.

(1) A cyclic static loading protocol is developed to induce random damage distribution, resolving the scale mismatch of traditional prefabricated crack models. The extent of sandstone fracture under explosive loads intensifies with the degree of damage. Specifically, the expansion range, width, and number of blast-induced cracks on the bottom surface, as well as the size of the blasting craters, increase as the degree of rock damage increases.
(2) A dual “gas-channeling and stress-synergy” mechanism is identified, demonstrating that blast gases preferentially propagate along pre-existing microcracks, enhancing energy efficiency. CT imaging reveals that the degree of damage, affected regions, crack size, and depth of penetration—all of which are aligned with the longitudinal axis of the sandstone—progressively increase with the degree of damage under explosive loads. These findings were corroborated by PFC-2D-based numerical simulations.
(3) A mesoscale PFC-2D model coupling damage evolution and blast dynamics is developed, reconstructing the full process from “static damage accumulation–stress wave propagation–macroscopic crack coalescence” at particle-scale resolution. High consistency between numerical simulations and CT observations validates multiscale analytical reliability.
(4) The theoretically predicted fracture radius of damaged sandstone under explosive loads was confirmed by experimental results, with discrepancies between theory and actual measurements under 5 % loading.
(5) The proposed damage-sensitive blasting parameter design framework significantly improves stability prediction accuracy in complex geological tunnels, offering critical theoretical support for directional blasting technologies and dynamic disaster prevention systems based on damage control strategies.

CRediT authorship contribution statement

Qiangqiang Zheng: Writing – original draft, Validation, Methodology, Funding acquisition, Formal analysis, Data curation, Conceptualization. **Pingfeng Li:** Resources, Investigation, Funding acquisition. **Ying Xu:** Supervision, Resources, Funding acquisition. **Bing Cheng:** Writing – review & editing, Visualization. **Hao Hu:** Validation, Methodology. **Hao Shi:** Validation, Methodology. **Shoudong Xie:** Investigation.

Declaration of competing interest

The authors declare that they have no known competing financial interests or personal relationships that could have appeared to influence the work reported in this paper.

Acknowledgement

This work was supported by the National Science and Technology Significant Special (No. 2024ZD1003406), Scientific Research Foundation for High-level Talents of Anhui University of Science and Technology (Grant No. 2023yjrc112), Foundation of Anhui Engineering Research Center of New Explosive Materials and Blasting Technology (No. AHBP2023B-06), Natural Science Research Project of Colleges and Universities in Anhui Province (No. 2024AH050374), Anhui Natural Science Foundation (No. 2408085QA029), Research Foundation for Postdoctoral of Anhui Province (Grant No. 2024B817), National Natural Science Foundation of China (Grant Nos. 52274071, 52404108).

References

[1] Hong Z, Tao M, Wu C, Zhou J, Wang D. The spatial distribution of excavation damaged zone around underground roadways during blasting excavation. Bull Eng Geol Environ 2023;82:155. https://doi.org/10.1007/s10064-023-03114-6.
[2] Yusoff IN, Ismail MAM, Tobe H, Date K, Yokota Y. Quantitative granitic weathering assessment for rock mass classification optimization of tunnel face using image analysis technique. Ain Shams Eng J 2023;14(1):101814. https://doi.org/10.1016/j.asej.2022.101814.
[3] Li C, Zhou J. Prediction and optimization of adverse responses for a highway tunnel after blasting excavation using a novel hybrid multi-objective intelligent model. Transp Geotech 2024;45:101228. https://doi.org/10.1016/j.trgeo.2024.101228.
[4] Shoeb M., Khan S.A., Alam T., Ali M.A., Gupta N.K., Ansari M.M., Kamal M.A., Shaik S., Eldin S.M., Dobrota D., Dynamic stability analysis of metro tunnel in layered weathered sandstone. Ain Shams Eng J, 15(1)(2024): 102258. https://doi.org/10.1016/j.asej.2023.102258.
[5] Huang J, Chen S, Liu M, Li K. Physical model test and numerical simulation study of cumulative damage to deep tunnel surrounding rock under cyclic blasting load. Int J Damage Mech 2023;32(2):161–84. https://doi.org/10.1177/10567895221133133.
[6] Ji L, Zhou C, Lu S, Jiang N, Gutierrez M. Numerical Studies on the Cumulative Damage Effects and Safety Criterion of a Large Cross-section Tunnel Induced by Single and Multiple Full-Scale Blasting. Rock Mech Rock Eng 2021;54:6393–411. https://doi.org/10.1007/s00603-021-02630-9.
[7] Zheng Q, Qan J, Zhang H, Chen Y, Zhang S. Velocity tomography of cross-sectional damage evolution along rock longitudinal direction under uniaxial loading. Tunn Undergr Sp Tech 2024;143:105503. https://doi.org/10.1016/j.tust.2023.105503.
[8] Zheng Q, Xu Y, Yin Z, Wang F, Zhang H. Dynamic tensile behaviour under impact loading for rocks damaged by static precompression. Archiv Civ Mech Eng 2023;23:199. https://doi.org/10.1007/s43452-023-00748-x.
[9] Lan R, Cheng R, Zhou Z, Chen L, Wang P, Wang Z. Damage and Fragmentation of Rock Under Multi-Long-Hole Blasting with Large Empty Holes. Rock Mech Rock Eng 2024;57:7603–22. https://doi.org/10.1007/s00603-024-03942-2.
[10] Talaat M, Yehia E, Mazek SA, Genidi MMM, Sherif AG. Finite element analysis of RC buildings subjected to blast loading. Ain Shams Eng J 2022;13(4):101698. https://doi.org/10.1016/j.asej.2021.101689.
[11] Dai L, Pan Y, Xiao Y, Wang A, Wang W, Wei C, et al. Parameter Design Method for Destressing Boreholes to Mitigate Roadway Coal Bursts: Theory and Verification. Rock Mech Rock Eng 2024. https://doi.org/10.1007/s00603-024-04042-x.
[12] Yang Y, Jiang N, Zhou C, Meng X, Zhu B, Cai Z. Damage analysis and safety control of surrounding rock around peripheral hole of diversion tunnel. Eng Fail Anal 2024;160:108226. https://doi.org/10.1016/j.engfailanal.2024.108226.
[13] Li X, Pan C, Li X, Shao C, Li H. Application of a synthetic rock mass approach to the simulation of blasting-induced crack propagation and coalescence in deep

fractured rock. Geomech Geophys Geo-Energ Geo-Resour 2022;8:57. https://doi.org/10.1007/s40948-022-00376-4.
[14] Chen M, Wei D, Yi C, Lu W, Johansson D. Failure mechanism of rock mass in bench blasting based on structural dynamics. Bull Eng Geol Environ 2021;80:6841–61. https://doi.org/10.1007/s10064-021-02324-0.
[15] Liu X, Yan P, Lu W, Zhu J, Zhang X, Lu A, et al. Investigation of dynamic crack formation mechanism based on a new crack dynamic driving model. Comput Geotech 2023;159:105471. https://doi.org/10.1016/j.compgeo.2023.105471.
[16] Liu K., Qiu T., Li X., Zhang X., Yang J., Song R., Li X., Deep Rock Blasting Using Decoupled Charge with Different Coupling Mediums. Int J Geomech 23(8)(2023): 04023112. https://ascelibrary.org/doi/abs/10.1061/IJGNAI.GMENG-8179.
[17] Mondal A, Pathrikar A, Karekal S. Phase-Field Based Peridynamics Implementation to Model Blast-Induced Fracture in Brittle Solids. Rock Mech Rock Eng 2024. https://doi.org/10.1007/s00603-024-03761-5.
[18] Fan LF, Wang LJ, Wu ZJ. An investigation of propagation direction induced difference of transmission coefficient in complex rock mass. Int J Rock Mech Min Sci 2020;135:104504. https://doi.org/10.1016/j.ijrmms.2020.104504.
[19] Ebrahim FS, Tan P, Ewan JS, Thomas RS. A review on the geotechnical design and optimisation of ultra-long ore passes for deep mass mining. Environ Earth Sci 2024; 83:301. https://doi.org/10.1007/s12665-024-11616-z.
[20] Chen D, Wang E, Li N. Study on the rupture properties and automatic identification model of micro-earthquakes and blasting events in a coal mine. Soil Dyn Earthq Eng 2021;146:106759. https://doi.org/10.1016/j.soildyn.2021.106759.
[21] Guo S, Zhang Q, He M, Seokwon J, Gao Y, Wang C. Crack Propagation Behavior and Damage Extent of Rock Mass under Instantaneous Expansion in Borehole. Rock Mech Rock Eng 2024;57:869–88. https://doi.org/10.1007/s00603-023-03584-w.
[22] Zhang Q, Ma C, Zhang XP, Liu Q, Qiu J, Liu D. Comparison of spatio-temporal characteristic of microseismic events in deep-buried tunnels with two excavation methods. Bull Eng Geol Environ 2024;83:81. https://doi.org/10.1007/s10064-024-03547-7.
[23] Li Z, Hu Y, Wang G, Zhou M, Hu W, Zhang X, et al. Study on cyclic blasting failure characteristics and cumulative damage evolution law of tunnel rock mass under initial in-situ stress. Eng Fail Anal 2023;150:107310. https://doi.org/10.1016/j.engfailanal.2023.107310.
[24] Yan G, Zhang F, Ku T, Hao Q, Peng J. Experimental Study and Mechanism Analysis on the Effects of Biaxial In-Situ Stress on Hard Rock Blasting. Rock Mech Rock Eng 2023;56:3709–23. https://doi.org/10.1007/s00603-022-03205-y.
[25] Fan Y., Miao X., Gao Q., Leng Z., Zheng J., Wu J., Influence of Water Depth on the Range of Crushed Zones and Cracked Zones for Underwater Rock Drilling and Blasting. Int J Geomech 22(10): 04022164. https://doi.org/10.1061/(ASCE)GM.1943-5622.0002485.
[26] Zuo J, Yang R, Gong M, Ge F. Effect of Different Filling Media Between Explosive and Blast-Hole Wall on Rock Blasting. Rock Mech Rock Eng 2023;56(2022): 5705–17. https://doi.org/10.1007/s00603-023-03366-4.
[27] Zhu Z, Fu T, Ning J, Li B. Mechanical behavior and constitutive model of frozen soil subjected to cyclic impact loading. Int J Impact Eng 2023;177:104531. https://doi.org/10.1016/j.ijimpeng.2023.104531.
[28] Ahn JK, Park D. Prediction of Near-Field Wave Attenuation Due to a Spherical Blast Source. Rock Mech Rock Eng 2017;50:3085–99. https://doi.org/10.1007/s00603-017-1274-3.
[29] Li Y, Zhu J, Han D, Zhao R, Ma Y, Zhou T. Experimental study of the dynamic responses of surrounding jointed rock masses and adjacent underground openings and induced ground vibrations subjected to underground explosion. Tunn Undergr Sp Tech 2023;13:105060. https://doi.org/10.1016/j.tust.2023.105060.
[30] Yan T, Li J, Li X. Dynamic viscoelastic model for rock joints under compressive loading. Int J Rock Mech Min Sci 2022;154:105123. https://doi.org/10.1016/j.ijrmms.2022.105123.
[31] Manatunga UI, Ranjith PG, De Silva VRS, Xu T, Zhang D. Evaluation of Slow-Releasing Energy Material (SREMA) Injection for In-Situ Rock Breaking Under Uniaxial and Triaxial Loading: An Experimental Study. Rock Mech Rock Eng 2024. https://doi.org/10.1007/s00603-024-03938-y.
[32] Dai J, Yang J, Yao C, Hu Y, Zhang X, Jiang Q, et al. Study on the mechanism of displacement mutation for jointed rock slopes during blasting excavation. Int J Rock Mech Min Sci 2022;150:105032. https://doi.org/10.1016/j.ijrmms.2021.105032.
[33] Li Q, Xu W, Wang K, Gao Z, Huo S, Huang C. Study on the mechanical behavior of crack propagation effect at the end of defect under explosive load. Int J Rock Mech Min Sci 2021;138:104624. https://doi.org/10.1016/j.ijrmms.2021.104624.
[34] Liu C, Yang M, Han H, Yue W. Numerical simulation of fracture characteristics of jointed rock masses under blasting load. Eng Computation 2019;36(6):1835–51. https://doi.org/10.1108/EC-09-2018-0404.
[35] Yu C, Yue H, Li H, Xia X, Liu B. Scale model test study of influence of joints on blasting vibration attenuation. Bull Eng Geol Environ 2021;80:533–50. https://doi.org/10.1007/s10064-020-01944-2.
[36] Tang ZC, Huang RQ, Liu QS, Wong LNY. Effect of contact state on the shear behavior of artificial rock joint. Bull Eng Geol Environ 2016;75:761–9. https://doi.org/10.1007/s10064-015-0776-z.
[37] Rashiddel A, Kharghani M, Dias D, Hajihassani M. Numerical study of the segmental tunnel lining behavior under a surface explosion – Impact of the longitudinal joints shape. Comput Geotech 128 2020:103822. https://doi.org/10.1016/j.compgeo.2020.103822.
[38] Liu J, He M, Guo S, Li J, Zhou P, Zhu Z. Study on characteristics of pressure relief by roof cutting under nonpillar-mining approach. Bull Eng Geol Environ 2022;81: 441. https://doi.org/10.1007/s10064-022-02943-1.
[39] Zheng Q, Xu Y, Yin Z, Wang F, Zhang H. Dynamic tensile behaviour under impact loading for rocks damaged by static precompression. Arch Civ Mech Eng 2023;23: 199. https://doi.org/10.1007/s43452-023-00748-x.
[40] Pei P, Dai F, Liu Y, Wei M. Dynamic tensile behavior of rocks under static pre-tension using the fattened Brazilian disc method. Int J Rock Mech Min Sci 2020; 126:104208. https://doi.org/10.1016/j.ijrmms.2019.104208.
[41] Dai J. Dynamic behaviours and blasting theory of rock. Beijing: Metallurgical Industry Press; 2013.
[42] Ni Y, Wang ZL, Li SY, Wang JG, Feng CC. Numerical study on the dynamic fragmentation of rock under cyclic blasting and different in-situ stresses. Comput Geotech 2024;172:106404. https://doi.org/10.1016/j.compgeo.2024.106404.
[43] Zhang G, Zhang S, Guo P, Wu S. Acoustic Emissions and Seismic Tomography of Sandstone Under Uniaxial Compression: Implications for the Progressive Failure in Pillars. Rock Mech Rock Eng 2023;56:1927–43. https://doi.org/10.1007/s00603-022-03155-5.
[44] Shi H, Zhang HQ, Song L, Yang Z, Wang Y. Failure characteristics of sandstone specimens with randomly distributed pre-cracks under uniaxial compression. Environ Earth Sci 2020;79:193. https://doi.org/10.1007/s12665-020-08933-4.
[45] Shi H, Chen W, Zhang H, Song L, Li M, Wu J, et al. Dynamic strength characteristics of fractured rock mass. Eng Fract Mech 2023;292:109678. https://doi.org/10.1016/j.engfracmech.2023.109678.
[46] Ríos-Bayona F, Johansson F, Mas-Ivars D, Sánchez-Juncal A, Bolin A. Using PFC^{2D} to simulate the shear behaviour of joints in hard crystalline rock. Bull Eng Geol Environ 2022;81:381. https://doi.org/10.1007/s10064-022-02885-8.
[47] Yu RG, Zhang ZH, Gao WL, Li CH, Wu C. Numerical simulation of rock mass blasting vibration using particle flow code and particle expansion loading algorithm. Simul Model Pract Th 2023;122:102686. https://doi.org/10.1016/j.simpat.2022.102686.
[48] Shoeb M, Khan SA, Alam T, Ali MA, Gupta NK, Ansari MM, et al. Dynamic stability analysis of metro tunnel in layered weathered sandstone. Ain Shams Eng J 2023;14 (1):102258. https://doi.org/10.1016/j.asej.2023.102258.
[49] Yan Z, Gong Y, Su H, Li P, Huang M, Yan D. Damage behavior of the surrounding medium caused by different blast-induced dynamic and static loadings. Eng Fract Mech 2024;309:110409. https://doi.org/10.1016/j.engfracmech.2024.110409.
[50] Feng CC, Wang ZL, Wang JG, Lu ZT, Li SY. A thermo-mechanical damage constitutive model for deep rock considering brittleness-ductility transition characteristics. J Cent South Univ 2024;31:2379–92. https://doi.org/10.1007/s11771-024-5700-x.
[51] Wang ZL, Ni Y, Wang JG, Li S. Improvement and performance analysis of constitutive model for rock blasting damage simulation. Simul Model Pract Th 2025;138:103043. https://doi.org/10.1016/j.simpat.2024.103043.
[52] Feng CC, Wang ZL, Wang JG, Fu JJ, Lu ZT. The mechanism of low strain rate and moderate principal stress effects in triaxial prestressed marble under lateral impulsive load. Soil Dyn Earthq Eng 2024;184:108860. https://doi.org/10.1016/j.soildyn.2024.108860.
[53] Wang SM, Wang ZL, Wang JG, Sun P. A Novel Dual-Scale Equivalent Model for Analyzing the Frequency Response of Wave Propagation in Jointed Rock Mass. Rock Mech Rock Eng 2024;57:9207–29. https://doi.org/10.1007/s00603-024-04078-z.

QiangqiangZheng is a lecturer at the School of Civil Engineering and Architecture, Anhui University of Science and Technology, China. His current research interests include blasting engineering, rock dynamics, and microseismic monitoring.

Pingfeng Li is a professor level senior engineer at Hongda Blasting Engineering Group Co., Ltd. He is also the director of the Key Laboratory of Safety and Intelligent Mining in Non coal Open pit Mines under the National Mine Safety Supervision Bureau. His current research interests include intelligent blasting in mines.

Ying Xu is a professor at the State Key Laboratory of Mining Response and Disaster Prevention and Control in Deep Coal Mines, Anhui University of Science and Technology, Vice President of the China Blasting Industry Association, and Chairman of the Anhui Engineering Blasting Association. His current research interests include blasting engineering and explosion and shock dynamics.

BingCheng is a lecturer at the Anhui Engineering Research Center of New Explosive Materials and Blasting Technology of Anhui University of Science and Technology. His current research interests include blasting engineering and explosion and shock dynamics.

Hao Hu is an experimentalist at the State Key Laboratory of Mining Response and Disaster Prevention and Control in Deep Coal Mines, Anhui University of Science and Technology. His current research interests include rock mechanics and microseismic monitoring.

Hao Shi is a lecturer at the School of Civil Engineering and Architecture, Anhui University of Science and Technology, China. His current research interests include rock mechanics and numerical simulation.

Shoudong Xie is the General Manager of Hongda Blasting Engineering Group Co., Ltd. His current research interests include intelligent blasting in mines.